UHASSELT
KNOWLEDGE IN ACTION

Maastricht University

Faculty of Medicine and Life Sciences
School for Life Sciences
Master of Biomedical Sciences

Master's thesis

Activity-dependent regulation of axon initial segment potassium channels

Sam Vanspauwen

Thesis presented in fulfillment of the requirements for the degree of Master of Biomedical Sciences, specialization Molecular Mechanisms in Health and Disease

SUPERVISOR :
Prof. dr. Jelle HENDRIX

SUPERVISOR :
Assoc. Prof. Hanne BORGER RASMUSSEN

2020
2021

Transnational University Limburg is a unique collaboration of two universities in two countries: the University of Hasselt and Maastricht University.

UHASSELT
KNOWLEDGE IN ACTION

www.uhasselt.be
Universiteit Hasselt
Campus Hasselt:
Martelarenlaan 42 | 3500 Hasselt
Campus Diepenbeek:
Agoralaan Gebouw D | 3590 Diepenbeek

Maastricht University

Faculty of Medicine and Life Sciences
School for Life Sciences
Master of Biomedical Sciences

Master's thesis

Activity-dependent regulation of axon initial segment potassium channels

Sam Vanspauwen

Thesis presented in fulfillment of the requirements for the degree of Master of Biomedical Sciences, specialization Molecular Mechanisms in Health and Disease

SUPERVISOR :

Prof. dr. Jelle HENDRIX

SUPERVISOR :

Assoc. Prof. Hanne BORGER RASMUSSEN

Activity-dependent regulation of axon initial segment potassium channels

Sam Vanspauwen[1], Jelle Hendrix[2], Hanne Borger Rasmussen[1]

[1] Membrane Trafficking Group, Department of Biomedical Sciences, The Faculty of Health and Medical Sciences, University of Copenhagen, Panum Institute, Blegdamsvej 3B, 2200 Copenhagen, Denmark
[2] Dynamic Bioimaging lab, Advanced Optical Microscopy Centre and Biomedical Research Institute, Universiteit Hasselt, Campus Diepenbeek, Agoralaan Gebouw C - B-3590 Diepenbeek, Belgium

To whom correspondence should be addressed:
Hanne Borger Rasmussen, Tel: +45 35 32 75 57; Email:hanneb@sund.ku.dk

Keywords: Axon initial segment, AIS plasticity, Voltage-gated potassium channels, Kv1.1, Kv2.1, Kv7.2, Superresolution microscopy, Stimulated emission depletion microscopy

ABSTRACT

Voltage-gated potassium channels critically impact action potential firing in our nervous system. Many of these channels like Kv1.1, Kv2.1, and Kv7.2 are located at the axon initial segment (AIS). Because of its high complexity and importance for action potential generation, the segment, and these potassium channels specifically, have been linked to many neurological disorders like ataxia and multiple types of epilepsy. In recent years, it was revealed that the AIS is susceptible to relocation and length alteration as a feedback mechanism to varying neuronal activity levels, referred to as AIS plasticity. However, It is currently unknown whether AIS potassium channels also experience relocation in this process. In this project, we performed confocal and stimulated emission depletion (STED) imaging on rat hippocampal neurons to uncover the effect of activity manipulation on AIS Kv1.1, Kv2.1, and Kv7.2. All examined potassium channels experienced a decreased expression after 48 hours of activity deprivation, indicating neurons limit their hyperpolarizing capability. However, nanoscale alterations were not observed. Interestingly, Kv2.1 was linked to a biphasic response, resulting from a rapidly increased cluster intensity, followed by an overall decreased number of clusters after prolonged activity deprivation. It was hypothesized that internal mechanisms attempt to traffic diffuse channels to the clusters where they become nonconducting, rapidly limiting their action potential inhibition. These results indicate that potassium channels are regulated by neuronal activity and subject to the mechanisms of AIS plasticity. Therefore, they proved to be compelling candidates for future research.

INTRODUCTION

The average human brain contains about 86 million densely compressed nerve cells, where each of these neurons contributes to the complex process of brain signaling. These endless cycles of neurons receiving synaptic inputs followed by action potential propagation through the axon to a downstream neuron are vital and ensure the normal functioning of almost every aspect of the body. This process is in part regulated by the axon initial segment (AIS). This 20-60 µm segment, located at the most proximal part of the axon, carries out two major functions. It acts as a barrier between the axon and cell body, thereby maintaining their molecular identity, and it ensures the correct relay of synaptic inputs into bursts of action potentials (1–3). The AIS is structurally composed of central microtubules and actin rings (**Figure 1**). These rings are periodically distributed along the axon in 190 nm intervals by beta-IV spectrin. On its membrane, the AIS expresses multiple types of sodium and potassium channels (**Figure 2**). Many of these ion channels are anchored to a specialized ankyrin/spectrin scaffold, connecting them to the cytoskeleton. Because of its essential role in this complex, Ankyrin G (AnkG) is often referred to as the "key organizer" of the AIS (2). AnkG is known to attach directly to spectrin tetramers and indirectly to the microtubule cytoskeleton via end binding (EB) proteins EB1 and EB3 (4). Even though spectrin seems to be part of the cytoskeleton and structurally independent of AnkG, recently, it was found that mutations in a specific subtype of AnkG prevent the recruitment of beta-IV spectrin to the AIS (5). Additionally, researchers found that AnkG is required to maintain the axo-dendritic polarity of mouse cerebellum neurons (6). These findings led to significant considerations about the importance of AnkG in the onset, development,

and regulation of the AIS.

On its membrane, the AIS holds multiple different types of voltage-gated sodium channels (Navs) and voltage-gated potassium channels (Kvs). Because the AIS is highly structured, these channels all exhibit a specific localization. Navs are generally known to be distributed over the entire AIS. However, Nav1.1 and Nav1.2 are located more proximally, whereas Nav1.6 is located more distally (7). These Navs have been shown to alternate with the actin rings due to their AnkG binding capability (8). In contrast, certain Kvs tend to be located more towards the distal AIS, as shown in previous research on Kv7.2 and Kv7.3 as well as Kv1.1 and Kv1.2 (9). These specific Kvs are located parallel to the actin ring, even though most possess an AnkG binding motif. Furthermore, in regards to Kv7.2 and Kv7.3, binding to AnkG is known to stabilize these channels at the AIS (10–13). It is currently unknown whether other mechanisms contribute to the localization and stability of these potassium channels at the AIS, and there are currently no binding partners known to facilitate the attachment of these channels to the actin rings. However, the involvement of postsynaptic density protein 93 (PSD-93) has been proposed as PSD-93 can impact Kv1 accumulation at the AIS (14). It should be noted that researchers were not able to replicate this effect *in vivo*. Lastly, Kv2.1 and Kv2.2 have not been linked to a specific AIS cytoskeleton-dependent localization. These channels are known to be located adjacent to GABAA receptors and appear to have an additional function besides contributing to action potential hyperpolarization (15). Recently, Kv2.1 and 2.2 have been associated with a more structural role in the AIS as they are able to form endoplasmic reticulum/plasma membrane junctions via interaction with VAMP-associated proteins (VAP), VAPA, and VAPB (16). Furthermore, these stable Kv2 cell surface clusters seem to be essential for membrane protein trafficking, including ion channel trafficking (17).

With the AIS being such an important and complex site in neurons, many human diseases like ataxia and multiple types of epilepsy have been associated with previously described potassium channels (18,19). Additionally, a wide range of disorders like bipolar disorder, autism, Alzheimer's, and multiple sclerosis have been associated with mutations or disrupted regulation of AnkG (20–26).

Further adding to its complexity, the AIS has been known to be dynamic under certain circumstances. This movability or AIS plasticity was first described in rat hippocampal neurons exposed to chronic depolarization with high potassium and shortly after in bird auditory neurons after auditory deprivation (27–29). These publications stated that the length of the AIS and its position varied in relation to the neurons' frequency tuning. This implied that the AIS distribution is optimally tuned to synaptic input, thus playing a critical role in regulating neuronal activity and function. In general, past research revealed that elevating neuronal activity in cultured hippocampal neurons leads to shortening and displacement of the AIS towards the distal axon, thereby lowering excitability. On the other hand, reducing neuronal activity leads to lengthening and displacement of the AIS towards the proximal axon, elevating excitability (30). It should be noted that certain aspects of this structural repositioning can take only hours, while other aspects can occur over the course of days (27,31). This slow

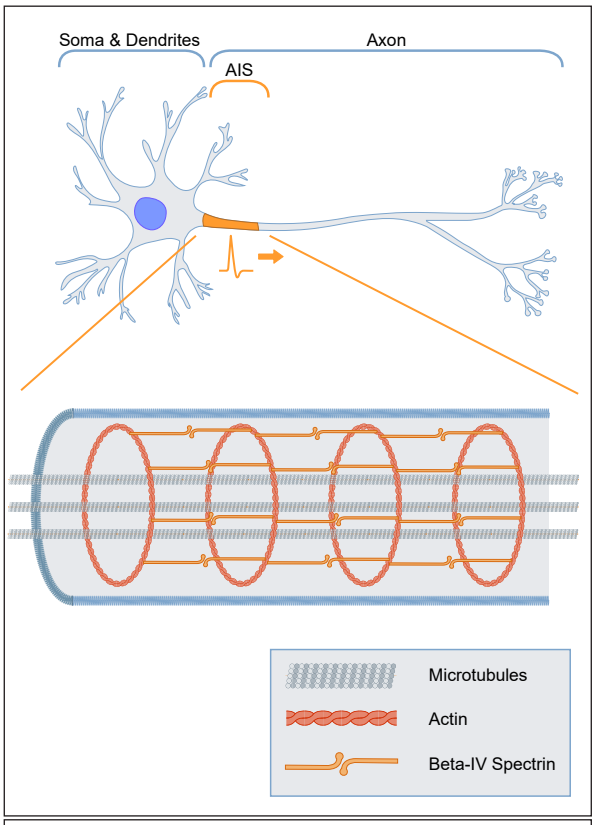

Figure 1: General location and cytoskeletal structure of the axon initial segment (AIS): Located at the most proximal part of the axon, the AIS contains a sturdy cytoskeletal structure composed of actin rings revolving around central microtubules. Actin rings are linked by Beta-IV spectrin structures.

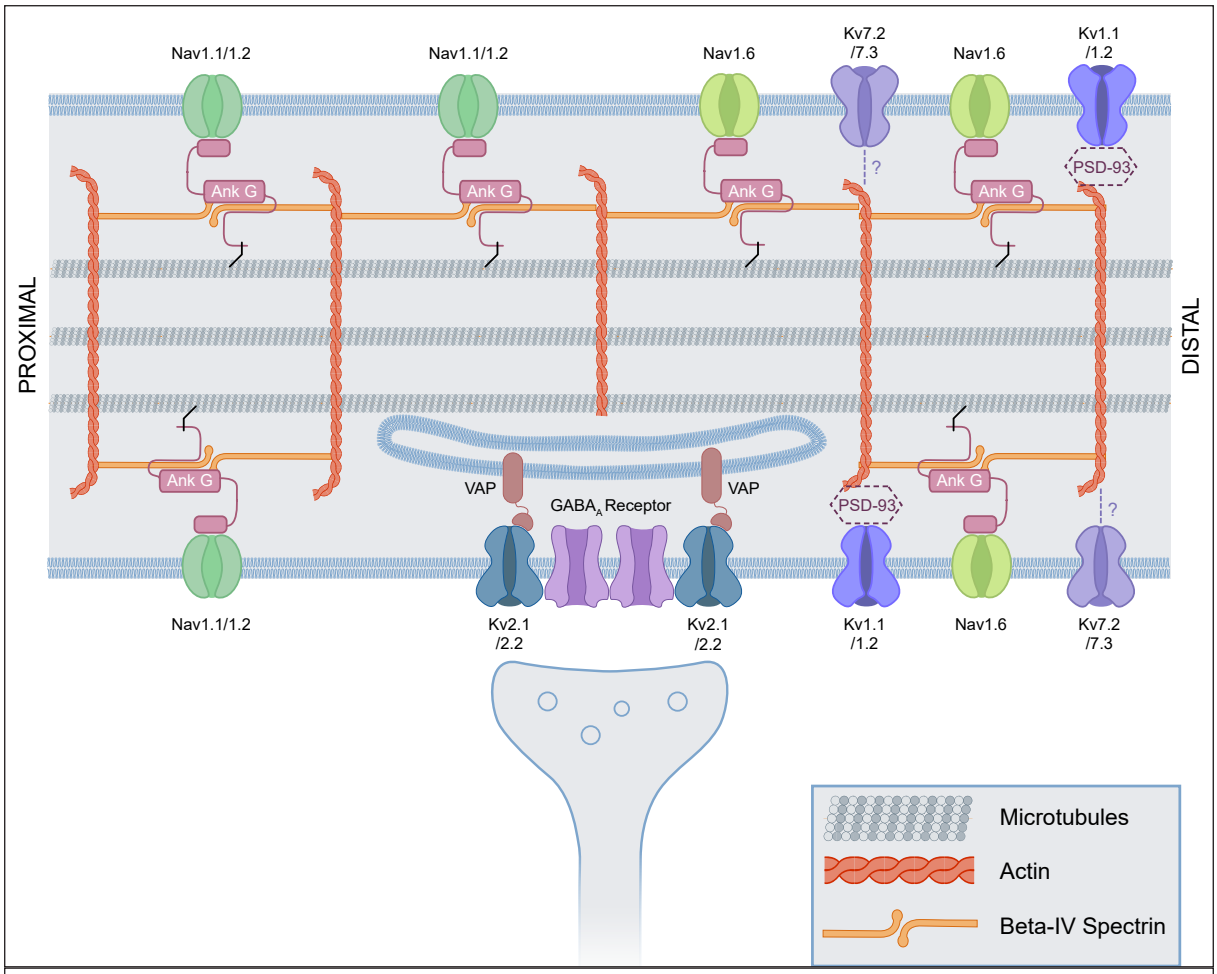

Figure 2: Graphical representation of the AIS: Ion channels in the AIS are attached to a sturdy cytoskeleton consisting of actin, beta-IV spectrin, and microtubules. Ankyrin G (AnkG) facilitates this attachment for sodium channels (Nav) while potassium channels (Kv) attach to the cytoskeleton via currently unknown mechanisms. However, PSD-93 has been hypothesized to be involved in the localization of Kv1.1/1.2 in some way. Kv2.1/2.1 are known to be located adjacent to GABAA receptors while being attached to intracellular cisternae via VAMP-associated proteins (VAPs). AnkG is attached directly to Navs and beta-IV spectrin while attached indirectly to the microtubules via end binding proteins EB1 and EB3 (black).

process to rearrange and disassemble the segment is not surprising, reinforcing notions of the AIS cytoskeleton's high stability and sturdiness (31).

In contrast to this general consensus on the relocation of the entire AIS, information on specific AIS ion channel relocations, especially potassium channels remains limited. Only recently, it was revealed that activity deprivation leads to decreased expression of Kv1.1 and increased expression of Kv7.2 in chick auditory neurons (32). It was hypothesized that interchanging these potassium channels could counteract activity alteration due to the kinetic differences between these potassium channel subtypes. Because channel-specific relocation over time remains to be further elucidated for both activity stimulation and deprivation, no concrete statements can be made on how these structural changes influence action potential strength and frequency. Furthermore, the mechanisms controlling these structural changes of AIS plasticity are currently unknown. However, some evidence indicates the possible involvement of Ca2+ signaling (27). Downstream cyclin-dependent kinase 5 (Cdk5) is known to promote Kv1 targeting to the AIS, while calmodulin regulates Kv7 channel assembly and clustering (31,33,34). Finally, the reorganization of cytoskeletal components might involve calpain, especially during neuronal injury (31,35).

Recently, researchers started making use of modern super-resolution microscopy techniques to uncover the nanoscale features of the AIS. Specifically, Stochastic Optical Reconstruction

Microscopy (STORM) and STimulated Emission Depletion (STED) microscopy have been the preferred methods for visualizing periodic structure in the segment but also the neuronal dendrites (36–38). While STORM is able to achieve higher spatial resolution, STED microscopy benefits from immediate image acquisition without the need for any additional data processing (39). STED microscopy still provides a spatial resolution well below the light diffraction limit by a simple but effective principle. In most typical STED microscopy implementations, this resolution is obtained by coaligining the Gaussian excitation beam of a scanning microscope with a second donut-shaped beam, called the STED laser. This beam is tuned in wavelength to de-excite fluorophores via stimulated emission, a process where far red-shifted depletion light can stimulate energy decay, causing the excited electron to drop to its ground state. This means that when both beams are focussed on the samples, there is a short temporal window where fluorophores within the donut-shaped STED beam are suppressed, allowing only the photons originating from the center to be detected (40,41).

This project aims to further examine a possible relocation of Kv1.1, Kv2.1, and Kv7.2 on a micro- and nanoscale. We hypothesize that these channels are subject to homeostatic plasticity. Furthermore, we hypothesize that ongoing microscale effects of activity manipulation coincide with nanoscale relocation of these potassium channels.

EXPERIMENTAL PROCEDURES

Neuronal cultures – Neuronal cultures were prepared from hippocampi isolated out of E18 rat embryos of either sex from pregnant Wistar rats as described previously (42). The protocol was carried out in accordance with the guidelines of the Danish Veterinary and Food Administration, Ministry of Environment and Food, and approved by the Department of Experimental Medicine at the University of Copenhagen. Isolated hippocampal neurons were cultured on an astroglial feeder layer prepared and cultured four days in advance in Minimum Essential Medium with horse serum (Thermo Fischer Scientific), 10 IU/ml penicillin-streptomycin (Thermo Fischer Scientific), and 0.5% (w/v) glucose (Thermo Fischer Scientific). After the addition of neurons, cells were left to grow in serum-free Neurobasal medium with B27 (Thermo Fischer Scientific), 0.5mM Glutamax (Thermo Fischer Scientific), and 10 IU/ml penicillin-streptomycin (Thermo Fischer Scientific)

Treatments – At 22 days *in vitro* (DIV), neurons were treated with either 1µM tetrodotoxin (TTX, for activity downregulation) or 20 µM bicuculine (BIC, for activity upregulation) by direct addition to the cell medium. Cells were incubated for 1, 6, 24, or 48 hours (these will be referred to as TTX1h, TTX6h, TTX24h, and TTX48h or BIC1h, BIC6h, BIC24h, and BIC48h in the rest of the paper) after which they were fixed. Per experiment, two coverslips with neurons were left untreated, where one was fixed at 22 DIV (CTRL22) and the other at 24 DIV (CTRL24).

Immunocytochemistry – Neurons were fixed in 2% paraformaldehyde in PBS for 2 minutes followed by 10 minutes in 100% methanol at -20°C. Unspecific binding was blocked for 30 minutes at room temperature with 0,2% fish skin gelatin in Phosphate-buffered saline (PBS) with 0,1% Triton X-100 (PBSTg). Next, neurons were incubated with primary antibodies diluted in PBSTg for one hour at room temperature. Primary antibodies used: mouse anti-Kv1.1 IgG2b (1:100 dilution, clone K36/15, NeuroMab), mouse anti-Kv2.1 IgG1 (1:100 dilution, clone K89/34, NeuroMab), rabbit anti-Kv7.2 (anti-KCNQ2, 1:100 dilution, Thermo Fisher Scientific), mouse anti-AnkG IgG2b (1:200 dilution, clone N106/65, NeuroMab), and rabbit anti-AnkG (1:500 dilution, SYSY). After washing, secondary antibodies diluted in PBSTg were added for 45 minutes at room temperature. Secondary antibodies used for confocal microscopy: goat anti-mouse IgG1 Alexa Fluor 488 (1:200 dilution, Thermo Fisher Scientific), goat anti-mouse IgG2b Alexa Fluor 555 (1:500 dilution, Thermo Fisher Scientific), goat anti-rabbit Alexa Fluor 568 (1:500 dilution, Thermo Fisher Scientific), goat anti-mouse IgG2b Alexa Fluor 647 (1:200 dilution, Thermo Fisher Scientific), and donkey anti-rabbit Alexa Fluor 647 (1:500 dilution, Thermo Fisher Scientific). Secondary antibodies for STED microscopy: goat anti-mouse STAR RED (1:200 dilution, Abberior), goat anti-rabbit STAR ORANGE (1:200 dilution, Abberior). After washing, coverslips were mounted on microscope slides using ProLong Diamond Antifade Reagent (Thermo Fisher Scientific).

Confocal microscopy and image analysis – A Zeiss LSM710 or LSM780 laser-scanning confocal microscope was used equipped with argon and helium-neon lasers and a 63x, 1.4 numerical aperture, oil-immersion objective. Images were taken in a 1024x1024 pixel format and a pinhole of 1 airy unit. Four-line averaging was used to reduce noise. Images were captured in Zeiss ZEN Blue 2011 or Zen Blue 2012 software and exported in .czi format, further analyzed in Fiji (Fiji_Is_Just_ImageJ). AnkG immunolabeling was used in all samples as a marker for the AIS. In each image, three one-pixel wide lines were drawn; a segmented line starting from the soma through the entire axon with a minimum distance of 60 µm, a segmented line of at least 10 µm drawn in a background region where no cells were included and a segmented line drawn in any of the dendrites of the same cell as the axonal line with a minimum distance of 20 µm. Fluorescence intensity profiles were extracted from each line, and the mean background value was subtracted. The axonal profile was smoothed using a 1.45 µm sliding mean. Mean AIS intensity (first 30µm of the axonal line), mean distal axon intensity (50-60 µm of the axonal line) and mean dendrite intensity (first 20 µm of dendrite line) were calculated, followed by calculation of AIS/dendrite and AIS/distal axon ratios.

The start, end, and length of the AIS as defined by AnkG were calculated based on the smoothed axonal line in which the average dendrite intensity was subtracted from every value (referred to as the axon-dendrite profile). AIS start is defined as the location where the axon-dendrite profile first reaches 33% of its max value in line with previous reports (27). AIS end was defined as the location where the axon-dendrite profile first dips below 33% of its max value after the AIS starting point. However, because AnkG can display gaps or irregularities in its staining, a limitation was implemented where the axon-dendrite profile has to dip below 33% of its max value for at least 3 µm to count as the AIS end. AIS length was defined as AIS end minus AIS start.

Intensity profiles, AIS/dendrite ratio, AIS/distal axon ratio, and the starting position for Kv1.1 and Kv7.2 staining were determined using the same method as AnkG. Additionally, the AIS density was determined by summating all intensity values between its starting and end positions, as defined by AnkG immunolabeling, divided by the length of this segment. For each experiment, this value was normalized by dividing each density value by the average density of CTRL22. Subsequently, the degree of decline of the end slope was calculated by fitting a function;

$$F(x) = S^{-x}$$

to a section of the axon-dendrite profile starting from the max value where S represents the steepness of the slope. Fitting was performed in Python 3.8 using the Lmfit library (43). The length of Kv1.1 and Kv7.2 segments were calculated with the start value defined as where the intensity profile first rises above 33%, and the end value defined as where the end slope dips below 0,33.

For Kv2.1 staining, the number of clusters, average cluster area, average cluster intensity, number of clusters relative to the AnkG area, and total cluster area relative to the AnkG area were calculated using in-house software (**Supplementary box 1**)

STED microscopy and image analysis – A Zeiss widefield microscopy attached to an Abberior STEDYCON STED system with a 63x, 1.4 numeric aperture objective was used for nanoscale super-resolution imaging. Images were taken with a 20 nm pixel size and variable pixel format using Abberior Software. A 561 nm excitation laser was used for imaging STAR ORANGE labeled AnkG, while a 640 nm excitation laser was used for imaging STAR RED labeled Kv1.1 or Kv2.1. Depletion of the signal was done by a 775 nm STED laser. For each Kv1.1 STED image, Fiji was used to extract a 5-pixel wide line profile of 2+ µm where clear periodicity was visible. Intensity profiles were further analyzed in Prism (GraphPad Software). Profiles were fitted to a sin wave

$$f(x) = Amplitude * \sin\left(\left(2\pi * \frac{x}{Frequency}\right) + Phase\ shift\right) + Height$$

with frequency, amplitude, height, and phase shift as variable parameters. A constraint was set on the fitting so that the Kv1.1 fit frequency and AnkG fit frequency was shared. The distance between Kv1.1 and AnkG peaks was extracted by calculating the minimum distance between the phase shifts of both fits.

Statistical analysis - For all data, outliers were removed using the ROUT method with a Q value of 1%. Conditions were compared using a Brown-Forsythe and Welch ANOVA test with multiple comparisons unless mentioned otherwise.

RESULTS AND DISCUSSION

Confocal microscopy revealed the subcellular localization of voltage-gated potassium channels – As a first step, we determined the subcellular localization of Kv1.1, Kv2.1, and Kv7.2 in 22 DIV rat hippocampal neurons (**Figure 3A-D**). Immunocytochemistry revealed that Kv1.1 and Kv7.2 had an even distribution that was increased in the distal AIS and faded out in the distal axon, Kv2.1 was expressed as clusters. These clusters were most intense in the AIS, especially the proximal AIS, but also present in the soma and proximal dendrites. These observations are in line with previous findings on these specific ion channels (9,16).

STED microscopy revealed the nanoscale distribution of Kv1.1 and Kv2.1 (**Figure 3E-G**). Kv1.1 exhibited a periodic structure similar to actin, beta4-spectrin, beta2-spectrin, and adducin (3,8,36,37). Kv2.1 clusters were, in some cases, circular in nature, possibly encompassing GABAA-receptors. AnkG mostly seemed to avoid the Kv2.1 clusters, sometimes forming circular shapes around Kv2.1 clusters (yellow arrows).

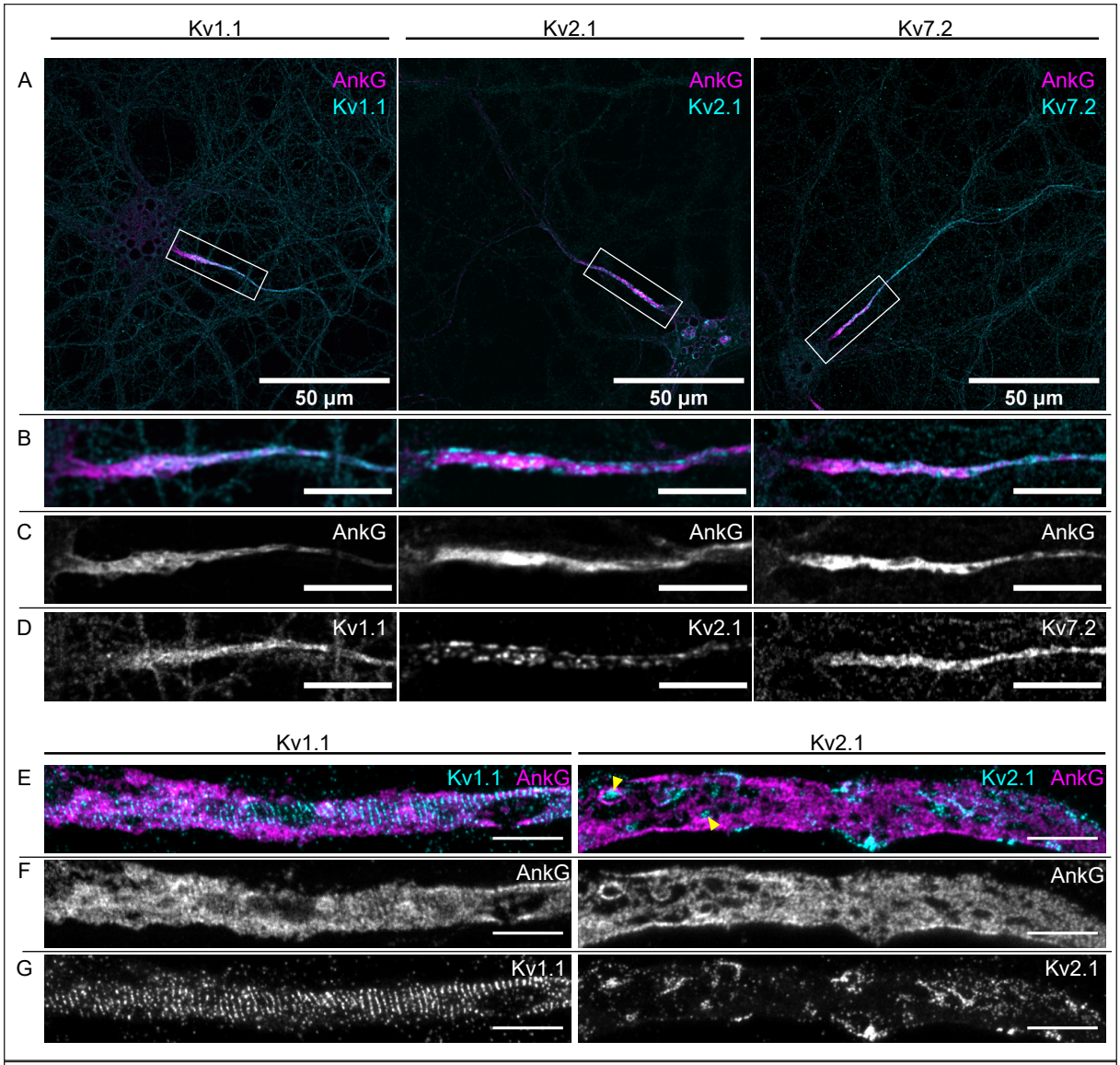

Figure 3: Subcellular localization of AIS voltage-gated potassium channels: A) Confocal images of 22 DIV rat hippocampal neurons stained for AnkG in magenta and Kv1.1, Kv2.1, and Kv7.2 (from left to right) in cyan. All potassium channels and AnkG showed an increased presence in the proximal axon, while Kv2.1 also showed slight clustering in the soma and proximal dendrites. B-D) Enlarged images of the AIS (white boxes in A). E) STED composite images of Kv1.1 and AnkG on the left and Kv2.1 and AnkG on the right. Kv1.1, Kv2.1, and their respective AnkG staining are separately visualized in F, and G. Scale bars represent a length of 50 µm in A, 10 µm in B, C, and D and 2µm in E, F, and G.

AnkG was also expected to be periodic, as shown previously (8); however, periodicity in the current samples was only mildly visible. This was mainly caused by three problems. AnkG was stained with a secondary Abberior STAR ORANGE antibody which has a 616 nm emission peak compared to STAR RED stained Kv1.1, which has a 655 nm emission peak. This means that AnkG emission was slightly further away from the 775 nm STED laser resulting in a resolution between 60 and 70 nm after imaging. In contrast, STAR RED could achieve resolutions up to 40 nm. Additionally, limitations of the microscope proved continuously challenging as Kv1.1 and AnkG had different focal plains in co-stained samples. After investigation, this was the result of a chromatic shift between the orange and red channels of about 80nm. Additionally, the used Kv1.1 antibody targeted an outer region of the potassium channel, while the used AnkG antibody targeted the internal C-terminal tail, resulting in an added biological shift. Finally, it is known that C-terminal targeted anti-AnkG antibody exhibits less profound periodicity (8).

Kv1.1 expression decreases gradually at the AIS during prolonged activity deprivation – To uncover the effect of activity regulation on Kv1.1, hippocampal neurons were treated with TTX for activity deprivation and BIC for activity stimulation. Confocal imaging revealed a gradual decrease in Kv1.1 AIS expression over the activity deprivation time series with TTX. A decrease in intensity was observed, especially after 24h and 48h of TTX administration to the cultures (TTX24h & TTX48h) (**Figure 4A**). These observations were supported by the intensity profiles of the time series (**Figure 4B**, left) and confirmed by statistical analysis of the normalized AIS densities (**Figure 4C**, left). Densities at TTX24h and TTX48h were significantly lower compared to control samples at 22 DIV (CTRL22) and 24 DIV (CTRL24). These findings indicate that hippocampal neurons downregulate Kv1.1 in response to activity deprivation. This suggests the cells possibly attempt to decrease overall activity by suppressing the hyperpolarizing capacity of Kv1.1. These results confirmed previous research from Kuba et. al. showing a decreased expression of Kv1.1 after 1, 3, 7, and 14+ days of activity deprivation (32). However, it should be noted that their method of activity deprivation did not involve TTX. Instead, their experiments were conducted on avian brainstem auditory neurons after auditory deprivation.

On the other hand, activity stimulation using BIC had no significant effect on the intensity of Kv1.1. Of note, a relatively large variation in normalized AIS density could be observed 48 hours after BIC administration (BIC48h) (**Figure 4C**, right). One explanation for this originated from the overall cell densities of the cultures. BIC data was derived for two separate hippocampal neuron cultures from which 15 cells from each of the six conditions were analyzed. It was noticed that the Kv1.1 intensity tended to go down in the low-density culture, while the opposite was observed in the high-density culture (**Supplement Figure 2**). However, some skepticism is needed before making any conclusions since CTRL24 data also varied between the cultures.

Activity deprivation impacts the localization of Kv1.1 – Besides the decrease in Kv1.1 intensity in the axon at 48h of activity deprivation, it became apparent that the Kv1.1 signal also got confined to a specific part of the AIS, whereas under normal conditions, Kv1.1 gradually disappeared in the distal axon (**Figure 4A**, left, TTX48h). This observation was supported by the intensity profiles where the end slope of the profile became steeper after prolonged activity deprivation (**Figure 5A**, left). End slope fitting to an exponentially decaying curve (S^{-x}) confirmed a steeper decay at 48 hours of activity deprivation (TTX48h)(**Supplement Figure 3**). This resulted in a slowly decreasing Kv1.1 segment length (**Figure 5B**). Additionally, a slight shift towards the distal axon was observed 1 hour after TTX treatment, indicating this potassium channel might have a rapid positional response to activity deprivation. However, this difference was only significant compared to CTRL24 and not CTRL22. In short, these results suggest that hippocampal neurons can alter the length, intensity, and location of Kv1.1 as a response to decreased overall activity levels.

Activity stimulation using BIC did not affect the length, start position, or end slope of Kv1.1 (**Figure 5B/C**, **Supplement Figure 3D**). However, a slight increase in length, as well as a small shift towards the distal axon, could be observed. Nevertheless, these variations were not significant and need confirmation by BIC experiment repetition.

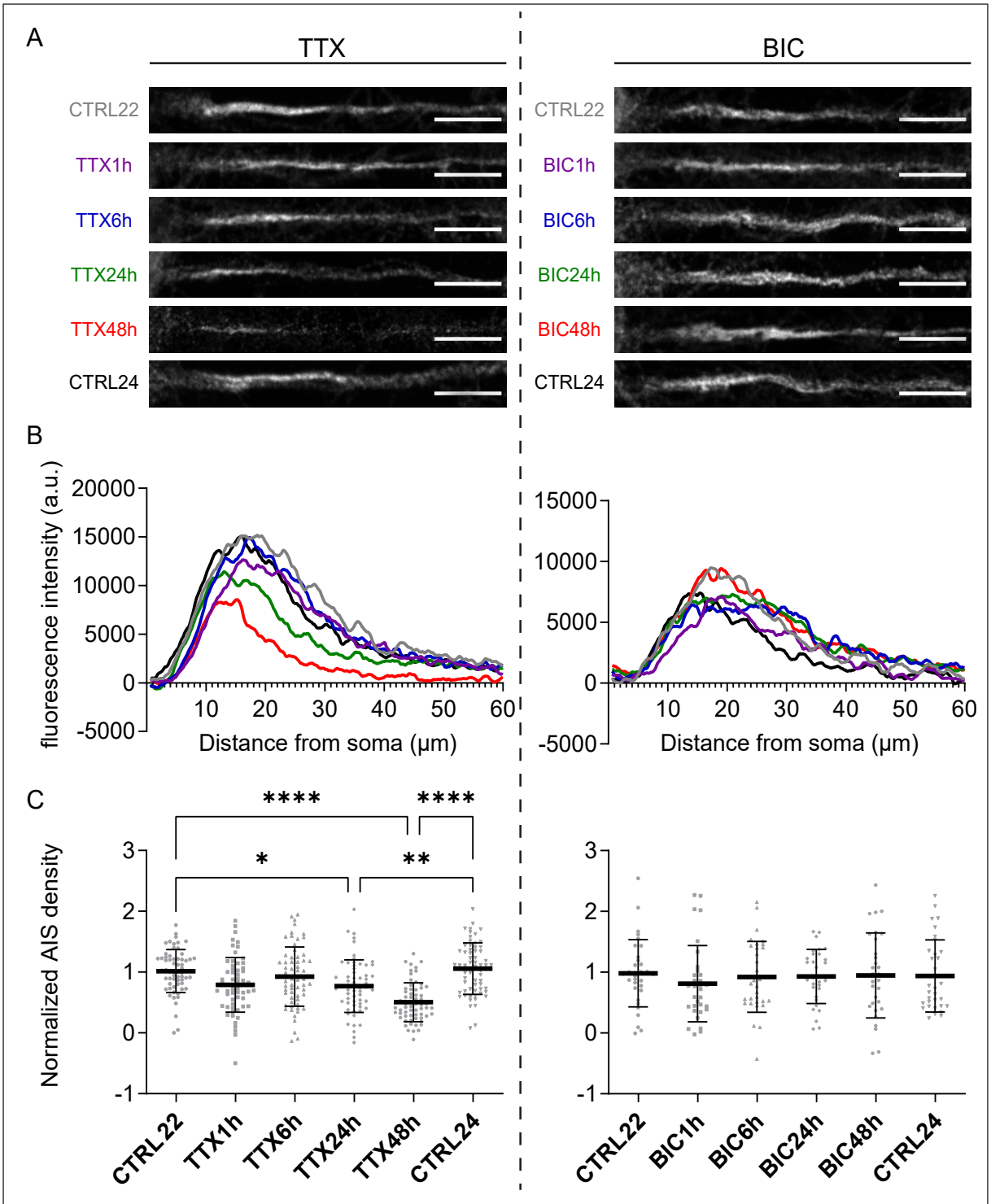

Figure 4: Effect of activity stimulation and deprivation on Kv1.1 expression: A) Enlarged confocal images of 22 DIV hippocampal neuron axons for each condition in a series of activity deprivation (TTX) and stimulation (BIC). B) Intensity profiles from the soma along the axon subtracted by the average intensity in the dendrite for each condition in an activity deprivation and stimulation time series. C) Normalized AIS density represents the average intensity over the calculated length of the AIS. Number of neurons; TTX time-series (n = 61-63 per condition), BIC time-series (n = 30-33 per condition). Scale bars represent a length of 10 µm. * $P < 0.05$, ** $P < 0.01$, **** $P < 0.0001$.

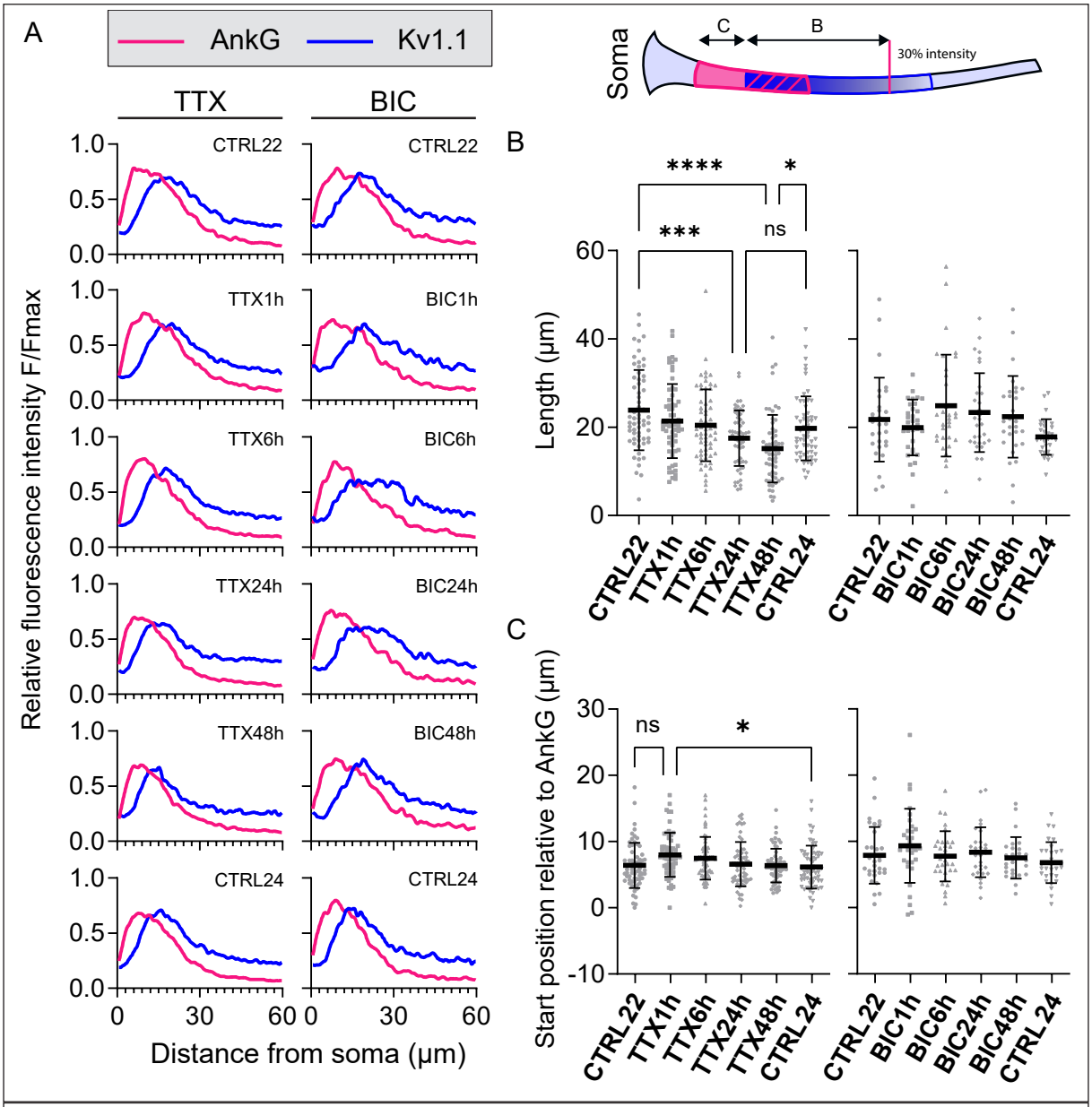

Figure 5: Effect of activity stimulation and deprivation on the localization of Kv1.1: A) Relative intensity profiles of AnkG (blue) compared to Kv1.1 (magenta) for each condition in an activity deprivation (TTX) and activity stimulation (BIC) time series. B) Length of the Kv1.1 segment where the start position is defined as the position where intensity rises above 33% of the max intensity for the first time, and the end position is defined as the position where a fitted end slope (S^{-x}) dips below 33% of the max intensity. C) Start position of Kv1.1 relative to the start position of AnkG along the axon. Number of neurons; TTX time-series (n = 61-63 per condition), BIC time-series (n = 30-33 per condition). * $P < 0.05$, *** $P < 0.001$, **** $P < 0.0001$.

No nanoscale changes to Kv1.1 periodicity were observed after activity manipulation – While Kv1.1 is prone to positional changes on a microscale, nanoscale analysis of hippocampal neurons after activity manipulation with TTX and BIC revealed no alterations to the characteristic periodicity of the channel (**Figure 6**). However, STED microscopy imaging did confirm an alternating Kv1.1 and AnkG periodicity (**Figure 6A**). It was found that Kv1.1 peaks exhibits a 190 nm frequency, similar to AnkG and actin (2) (**Figure 6B**), while the distance between Kv1.1 and AnkG was close to half of 190 nm, confirming alternating periodicity (**Figure 6C**). These observations remained unchanged after short-term (TTX1h, BIC1h) and long-term (TTX48h, BIC48h) activity manipulation. It should be noted that these results do not entirely eliminate the

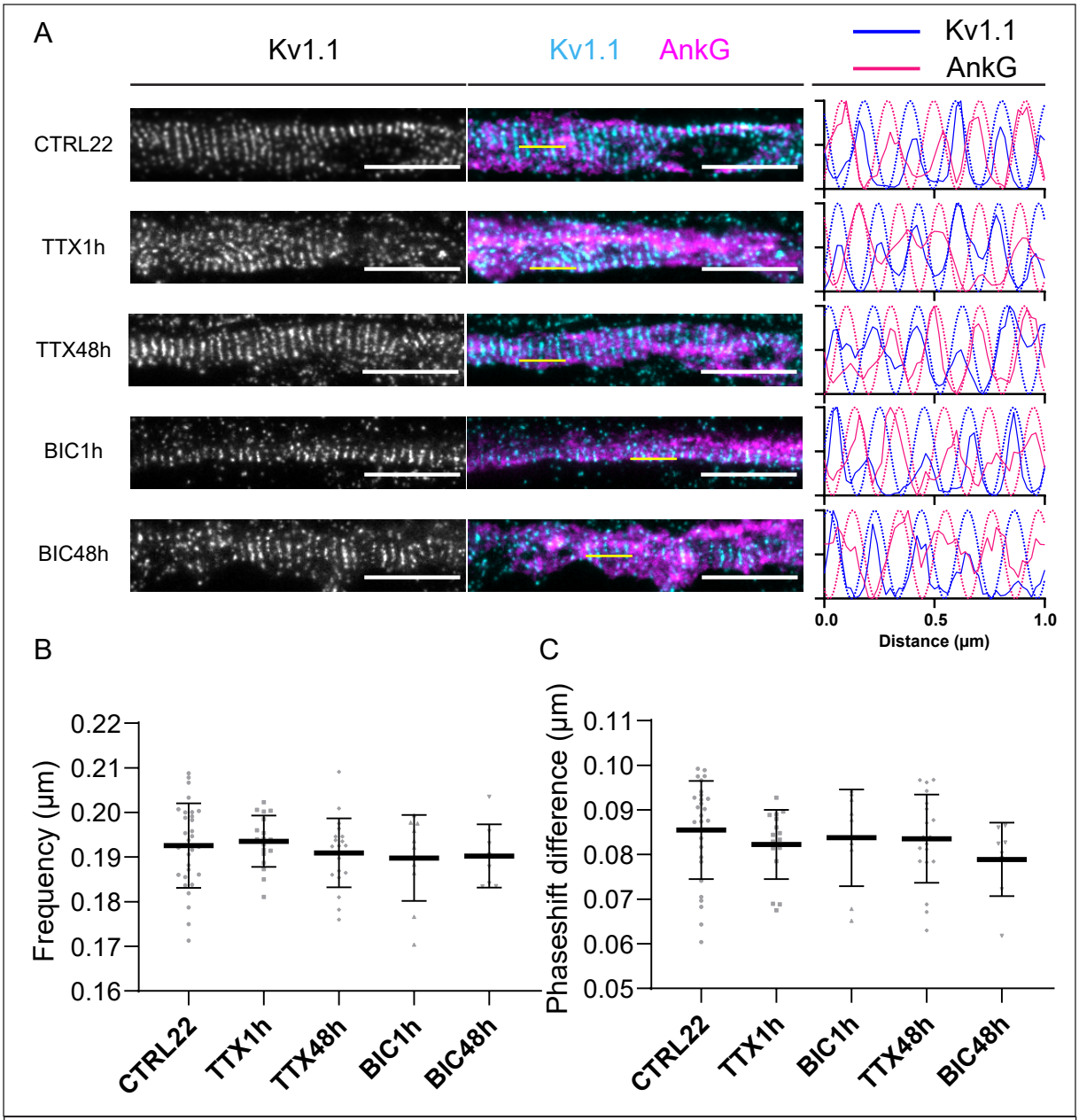

Figure 6: Nanoscale effects of activity manipulation on Kv1.1: A) STED microscopy images of rat hippocampal neuron AIS Kv1.1 after short- (TTX1h, BIC1h) and long-term (TTX48h, BIC48h) activity manipulation. Kv1.1 images are displayed on the left, while composite images with AnkG are displayed in the middle. Intensity profiles of a 1 µm line (yellow) and their respective fitted sin wave (dashed line) are displayed on the right and show an alternating periodicity between Kv1.1 and AnkG. B) Frequencies of the Kv1.1 fitted sin waves. No significance was observed. C) Phaseshift difference between Kv1.1 and AnkG or, in other words, the minimum distance between Kv1.1 and AnkG peaks. No significance was observed. Number of neurons; CTRL22 (n = 30), TTX conditions (n = 20 per condition), BIC conditions (n = 8-10). Scale bars represent a length of 2 µm.

possibility of nanoscale relocalization of Kv1.1. As previously mentioned, this potassium channel has an AnkG binding site while exhibiting no actual colocalization with AnkG. Hence, it was expected that colocalization would be observed upon manipulating activity. However, the used methodology only confirmed that no colocalization with AnkG occured in areas where apparent Kv1.1 periodicity was observed. This means K1.1/AnkG colocalization could still occur in areas where Kv1.1 experienced a more diffuse localization. Other analysis techniques besides sin wave-fitting would be needed to determine this. In the future, it would be beneficial to use techniques like

autocorrelation to obtain a degree of periodicity for both Kv1.1 and AnkG, while cross-correlation and another adequate correlation techniques could indicate Kv1.1/AnkG colocalization in the more diffuse regions of the AIS.

Kv2.1 expression was decreased after activity deprivation – Next, we analyzed Kv2.1 using the same microscopy techniques as Kv1.1. However, because of its clustering nature, a different approach was taken for the analysis. Confocal microscopy revealed downregulation of Kv2.1 clusters after prolonged activity deprivation (**Figure 7A**, TTX24h, TTX48h). It was confirmed by image analysis that cluster density was significantly lower after 24 hours, compared to the 24 DIV control, and after 48 hours compared to both controls (**Figure 7B**, left). Furthermore, analysis of the properties of each cluster revealed an increased cluster fluorescence intensity at 1, 6, and 24 hours post-activity deprivation (**Figure 7C**, left) while the average cluster area was not altered between conditions (**Supplement Figure 4A**, left). These findings indicate that Kv2.1 experienced both rapid and long-term alterations to its positioning and expression in activity-deprived neurons. Similar to Kv1.1, it was not surprising that neurons want to downregulate the hyperpolarizing capability of this channel by decreasing its expression after long-term activity deprivation. In contrast, a rapid increase in cluster intensity was not expected. However, this phenomenon was quickly clarified by previous research on the characteristics of Kv2.1. O'Connell et. al. stated in a 2010 research paper that cell-attached patch-clamp indicated that Kv2.1 clusters are nonconducting while whole-cell Kv2.1 current is likely derived from nonclustered diffuse channels (44). This means hippocampal neurons likely rapidly inactivate Kv2.1 by trafficking diffuse channels to the clusters indicated by the intensity increase inside the clusters. Subsequently, the cell decreases the overall surface-expression of clustered Kv2.1, indicated by the decrease in cluster density. It should be noted that the rapid cluster intensity increase was not significant compared to the 24 DIV control (**Figure 7C**, left). However, it is unlikely that this short-term phenomenon was caused purely by the aging and maturation of the cell culture rather than the influence of TTX.

Cells treated with BIC also showed decreased cluster density after 24 hours of treatment (**Figure 7B**, right). However, because this was no longer the case after 48 hours of treatment, no significant difference was observed with CTRL24, and the variance of this condition was relatively large; more repetitions of this experiment are needed to confirm this. A slow decrease in cluster area and cluster fluorescence intensity was observed after 48 hours of activity stimulation (**Figure 7C**, **Supplement Figure 4**). This could indicate that the cell now reacted to increased overall activity by trafficking Kv2.1 channels out of the clusters, making them active. However, because these conditions were not significantly different from CTRL24, this response might be unrelated to BIC treatment but due to the maturation of the culture.

STED microscopy revealed nanoscale structural changes to Kv2.1 clusters – Activity deprivation time-series confirmed previous confocal microscopy results showing a decreased number of clusters after 48 hours of TTX treatment (**Figure 8**). Another noticeable characteristic of Kv2.1 clusters at TTX48h was that almost all clusters lost their circular pattern.

BIC experiments showed high variability and inconsistent results – Besides the previously discussed difference in culture density and overall few experiment repetitions, one of the theories explaining high variability in activity stimulation experiments related to the function of BIC itself. Since this substance blocks GABAA receptors, it could be expected that BIC would have a more significant effect when there are more cells and synapses compared to low-density cultures with fewer cells and synapses, making BIC experiments inconsistent when cell culture density varied among repetitions. Additionally, it is known that GABAergic synapses are not always hyperpolarizing. Specifically, researchers found that GABAA receptor-mediated responses are often depolarizing during early neuronal development, a phenomenon mediated by the neuronal (Cl-)-extruding K+/Cl- co-transporter KCC2 (45,46). In the future, it might be advisable to repeat BIC experiments with other activity stimulating substances like KCl (47).

Kv7.2 reacted similarly to activity deprivation compared to Kv1.1 – Confocal microscopy revealed a visibly noticeable decrease in Kv7.2 expression upon prolonged activity deprivation (**Figure 9A**), also represented in the fluorescence intensity profiles (**Figure 9B**). Calculating the

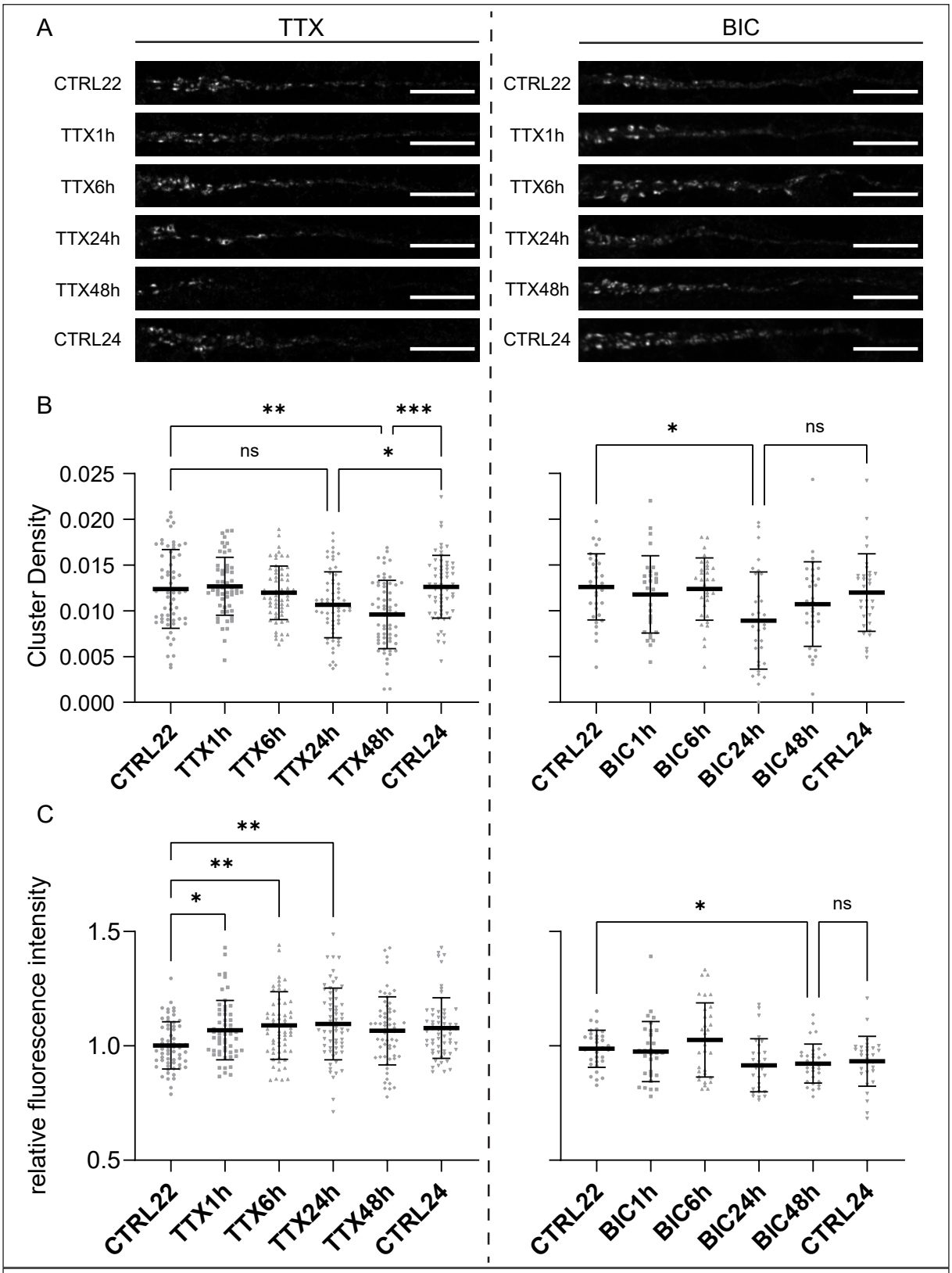

Figure 7: Effect of activity manipulation on Kv2.1 clusters: A) Confocal microscopy images of rat hippocampal neuron AIS Kv2.1 after multiple periods of activity deprivation (TTX) or simulation (BIC). B) Cluster density, or the number of clusters per area unit, after a time series of TTX or BIC treatment. C) Relative fluorescence intensity, meaning the average cluster intensity relative to CTRL22. Number of neurons; TTX time-series (n = 58-62 per condition), BIC time-series (n = 30-33). Scale bars represent a length of 10 μm. * $P < 0.05$, ** $P < 0.01$, *** $P < 0.001$.

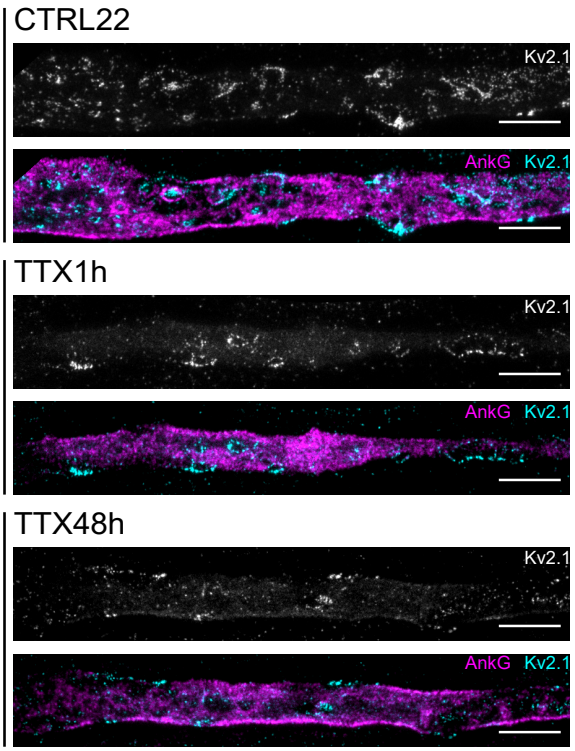

Figure 8: Nanoscale effects of activity deprivation on AIS Kv2.1: A) STED microscopy image of rat hippocampal neuron AIS Kv2.1 after short- (TTX1h) and long-term (TTX48h) activity deprivation including a control image at 22 DIV (CTRL22). Scale bars represent a length of 2 µm.

normalized Kv7.2 density and statistical analysis confirmed a significantly decreased expression at TTX48h (**Figure 9C**). This suggests that similar to Kv1.1, hippocampal neurons are also able to reduce the number of Kv7.2 channels in the AIS as a feedback mechanism to deprived overall activity. These findings contrasted previous results from Kuba e.a., stating that Kv7.2 expression was increased post-activity deprivation (32). However, like discussed previously, they used chick auditory neurons compared to rat hippocampal neurons and had a different approach to deprive activity. However, this does suggest that AIS plasticity varies between different regions of the brain.

Kv7.2 exhibited a distal shift at TTX1h compared to CTRL24, similar to Kv1.1 (**Supplement Figure 5A**). Since no significance was detected when comparing this condition to CTRL22, this observation could be related to the culture's age. No activity deprivation-dependent alterations were found relating to the length or steepness of Kv7.2's end slope (**Supplement Figure 5B,C**). However, Images and end slope

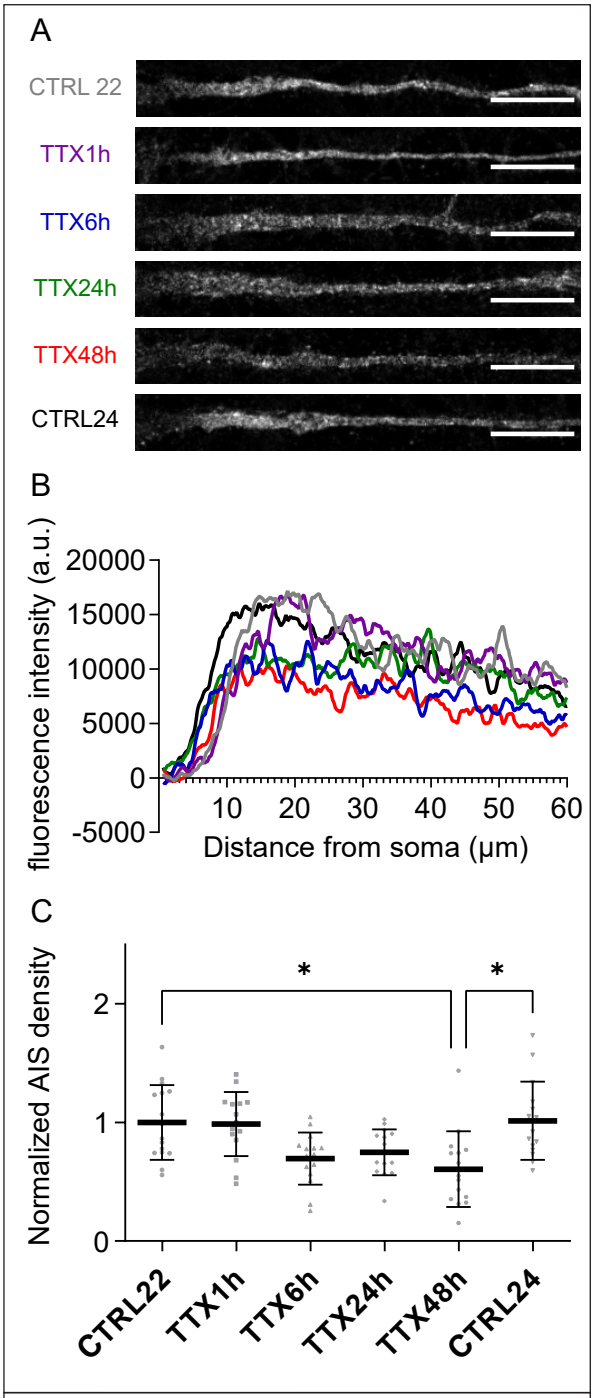

Figure 9: Effect of activity manipulation on Kv7.2 expression: A) Confocal microscopy images of rat hippocampal neuron AIS Kv7.2 after activity deprivation (TTX). B) Intensity profiles of Kv7.2 from the soma along the axon subtracted by the average intensity in the dendrite for each condition in an activity deprivation time series. C) Normalized AIS density represents the intensity over the calculated length of the AIS. Number of neurons; TTX time-series (n = 15-16 per condition). Scale bars represent a length of 10 µm. * $P < 0.05$.

fitting did indicate a much flatter end slope compared to Kv1.1, meaning Kv7.2 has a more profound presence in the distal axon than Kv1.1.

Unfortunately, no activity stimulation or STED experiments were performed on Kv7.2 because of unforeseen problems with the used antibody. While repeating TTX time-series experiments with a new batch of the anti-Kv7.2 Thermo Fisher Scientific antibody, it was noticed that the staining was not as intense as the previous batch (**Supplement Figure 6A**). Even more noticeable was the unexplainable effect this antibody had on the same anti-AnkG antibody that was used in previous experiments (**Supplement Figure 6B**). While it was attempted to optimize another anti-Kv7.2 antibody from SYSY, it never achieved the same quality as the initial Thermo Fisher Scientific antibody. Additionally, this antibody did not exhibit any periodicity in STED microscopy images.

CONCLUSTION

Confocal microscopy provided a strong indication that rat hippocampal neurons are capable of suppressing Kv1.1 and Kv7.2 expression after activity deprivation. Additionally, these cells are able to decrease the length of the Kv1.1 segment, confining this channel to a specific part of the distal AIS. This indicates that these cells have internal mechanisms to suppress the hyperpolarizing capacity of these potassium channels when the overall activity level of the cell is decreased. These findings further amplify previous notions of AIS plasticity being a feedback mechanism to keeps overall action potential strength stable despite external stimuli. While Kv2.1 distribution is visually entirely different for the previously mentioned potassium channels because of its clustering nature, it was similarly affected by activity deprivation. Despite the cluster intensity not decreasing, the number of clusters dropped significantly after 48 hours of TTX treatment. This indicated that hippocampal neurons are able to suppress the overall presence of Kv2.1 when affected by decreased activity levels. More interestingly, Kv2.1 exhibited a rapid response following activity deprivation indicated by an increased cluster intensity already after 1 hour of TTX treatments. It was hypothesized that this might be an acute mechanism to stabilize the cell's activity level by trafficking active diffused Kv2.1 channels, turning them into inactive clustered Kv2.1 channels. STED microscopy proved to be an effective, fast, and easy-to-use technique to visualize Kv1.1 periodicity and Kv2.1 circular clusters. While sin wave fitting was sufficient to prove non-varying Kv1.1 periodicity and localization post-activity-regulation, more specialized correlation techniques are needed to further analyze the colocalization of potassium channels with AnkG and other potential proteins. In conclusion, this project revealed that neuronal activity alterations are able to regulate AIS localized Kv1.1, Kv2.1, and Kv7.2. While AIS Kv2.1 has received limited interest in the past, we highlighted the complexity of the short- and long-term Kv2.1 alterations making this an extremely interesting target for further examination. In the future, investigation of all these potassium channels in both healthy and pathological conditions will be needed to uncover the underlying pathways driving this plasticity and potentially finding drug targets for numerous diseases. Nevertheless, this research emphasizes the intricacy and importance of AIS plasticity to stabilize neuron firing in our nervous system.

REFERENCES

1. Rasband MN. The axon initial segment and the maintenance of neuronal polarity. Nat Rev Neurosci. 2010 Aug;11(8):552–62.
2. Leterrier C. The Axon Initial Segment, 50Years Later. In: Current Topics in Membranes [Internet]. Elsevier; 2016 [cited 2021 Jun 28]. p. 185–233. Available from: https://linkinghub.elsevier.com/retrieve/pii/S1063582315000691
3. Leterrier C. The Axon Initial Segment: An Updated Viewpoint. J Neurosci. 2018 Feb 28;38(9):2135–45.
4. Freal A, Fassier C, Le Bras B, Bullier E, De Gois S, Hazan J, et al. Cooperative Interactions between 480 kDa Ankyrin-G and EB Proteins Assemble the Axon Initial Segment. J Neurosci. 2016 Apr 20;36(16):4421–33.

5. Yang R, Walder-Christensen KK, Lalani S, Yan H, García-Prieto ID, Álvarez S, et al. Neurodevelopmental mutation of giant ankyrin-G disrupts a core mechanism for axon initial segment assembly. Proc Natl Acad Sci. 2019 Sep 24;116(39):19717–26.
6. Sobotzik J-M, Sie JM, Politi C, Del Turco D, Bennett V, Deller T, et al. AnkyrinG is required to maintain axo-dendritic polarity *in vivo*. Proc Natl Acad Sci. 2009 Oct 13;106(41):17564–9.
7. Van Wart A, Trimmer JS, Matthews G. Polarized distribution of ion channels within microdomains of the axon initial segment. J Comp Neurol. 2007 Jan 10;500(2):339–52.
8. Leterrier C, Potier J, Caillol G, Debarnot C, Rueda Boroni F, Dargent B. Nanoscale Architecture of the Axon Initial Segment Reveals an Organized and Robust Scaffold. Cell Rep. 2015 Dec;13(12):2781–93.
9. Battefeld A, Tran BT, Gavrilis J, Cooper EC, Kole MHP. Heteromeric Kv7.2/7.3 Channels Differentially Regulate Action Potential Initiation and Conduction in Neocortical Myelinated Axons. J Neurosci. 2014 Mar 5;34(10):3719–32.
10. Cooper EC. Made for "anchorin": Kv7.2/7.3 (KCNQ2/KCNQ3) channels and the modulation of neuronal excitability in vertebrate axons. Semin Cell Dev Biol. 2011 Apr;22(2):185–92.
11. San-Cristobal P, Lainez S, Dimke H, de Graaf MJJ, Hoenderop JGJ, Bindels RJM. Ankyrin-3 is a novel binding partner of the voltage-gated potassium channel Kv1.1 implicated in renal magnesium handling. Kidney Int. 2014 Jan;85(1):94–102.
12. Barry J. Ankyrin-G Directly Binds to Kinesin-1 to Transport Voltage-Gated Na+ Channels into Axons. Dev Cell. :15.
13. Benned-Jensen T, Christensen RK, Denti F, Perrier J-F, Rasmussen HB, Olesen S-P. Live Imaging of Kv7.2/7.3 Cell Surface Dynamics at the Axon Initial Segment: High Steady-State Stability and Calpain-Dependent Excitotoxic Downregulation Revealed. J Neurosci. 2016 Feb 17;36(7):2261–6.
14. Ogawa Y, Horresh I, Trimmer JS, Bredt DS, Peles E, Rasband MN. Postsynaptic Density-93 Clusters Kv1 Channels at Axon Initial Segments Independently of Caspr2. J Neurosci. 2008 May 28;28(22):5731–9.
15. Misonou H, Thompson SM, Cai X. Dynamic Regulation of the Kv2.1 Voltage-Gated Potassium Channel during Brain Ischemia through Neuroglial Interaction. J Neurosci. 2008 Aug 20;28(34):8529–38.
16. Kirmiz M, Vierra NC, Palacio XS, Trimmer XJS. Identification of VAPA and VAPB as Kv2 Channel-Interacting Proteins Defining Endoplasmic Reticulum–Plasma Membrane Junctions in Mammalian Brain Neurons. :23.
17. Deutsch E, Weigel AV, Akin EJ, Fox P, Hansen G, Haberkorn CJ, et al. Kv2.1 cell surface clusters are insertion platforms for ion channel delivery to the plasma membrane. Martin TFJ, editor. Mol Biol Cell. 2012 Aug;23(15):2917–29.
18. Rasmussen HB, Trimmer JS. The Voltage-Dependent K+ Channel Family. In: Bhattacharjee A, editor. The Oxford Handbook of Neuronal Ion Channels [Internet]. Oxford University Press; 2019 [cited 2020 Oct 18]. Available from: https://oxfordhandbooks.com/view/10.1093/oxfordhb/9780190669164.001.0001/oxfordhb-9780190669164-e-1
19. Döring JH, Schröter J, Jüngling J, Biskup S, Klotz KA, Bast T, et al. Refining Genotypes and Phenotypes in KCNA2-Related Neurological Disorders. Int J Mol Sci. 2021 Mar 10;22(6):2824.
20. Sun X, Wu Y, Gu M, Liu Z, Ma Y, Li J, et al. Selective filtering defect at the axon initial segment in Alzheimer's disease mouse models. Proc Natl Acad Sci. 2014 Sep 30;111(39):14271–6.
21. Tsushima H, Emanuele M, Polenghi A, Esposito A, Vassalli M, Barberis A, et al. HDAC6 and RhoA are novel players in Abeta-driven disruption of neuronal polarity. Nat Commun. 2015 Nov;6(1):7781.
22. Hamada MS, Kole MHP. Myelin Loss and Axonal Ion Channel Adaptations Associated with Gray Matter Neuronal Hyperexcitability. J Neurosci. 2015 May 6;35(18):7272–86.
23. Benusa SD, George NM, Sword BA, DeVries GH, Dupree JL. Acute neuroinflammation induces AIS structural plasticity in a NOX2-dependent manner. J Neuroinflammation. 2017 Dec;14(1):116.
24. Kloth K, Denecke J, Hempel M, Johannsen J, Strom TM, Kubisch C, et al. First de novo ANK3 nonsense mutation in a boy with intellectual disability, speech impairment and autistic features. Eur J Med Genet. 2017 Sep;60(9):494–8.

25. Lopez AY, Wang X, Xu M, Maheshwari A, Curry D, Lam S, et al. Ankyrin-G isoform imbalance and interneuronopathy link epilepsy and bipolar disorder. Mol Psychiatry. 2017 Oct;22(10):1464–72.
26. Zhu S, Cordner ZA, Xiong J, Chiu C-T, Artola A, Zuo Y, et al. Genetic disruption of ankyrin-G in adult mouse forebrain causes cortical synapse alteration and behavior reminiscent of bipolar disorder. Proc Natl Acad Sci. 2017 Sep 26;114(39):10479–84.
27. Grubb MS, Burrone J. Activity-dependent relocation of the axon initial segment fine-tunes neuronal excitability. Nature. 2010 Jun;465(7301):1070–4.
28. Kuba H, Oichi Y, Ohmori H. Presynaptic activity regulates Na+ channel distribution at the axon initial segment. Nature. 2010 Jun;465(7301):1075–8.
29. Kuba H. Structural tuning and plasticity of the axon initial segment in auditory neurons: Tuning and plasticity of the AIS. J Physiol. 2012 Nov 15;590(22):5571–9.
30. Yamada R, Kuba H. Structural and Functional Plasticity at the Axon Initial Segment. Front Cell Neurosci [Internet]. 2016 Oct 25 [cited 2021 Jul 10];10. Available from: http://journal.frontiersin.org/article/10.3389/fncel.2016.00250/full
31. Chang K-J, Rasband MN. Excitable Domains of Myelinated Nerves. In: Current Topics in Membranes [Internet]. Elsevier; 2013 [cited 2020 Sep 28]. p. 159–92. Available from: https://linkinghub.elsevier.com/retrieve/pii/B9780124170278000052
32. Kuba H, Yamada R, Ishiguro G, Adachi R. Redistribution of Kv1 and Kv7 enhances neuronal excitability during structural axon initial segment plasticity. Nat Commun [Internet]. 2015 Nov 19 [cited 2020 Oct 23];6. Available from: https://www.ncbi.nlm.nih.gov/pmc/articles/PMC4673506/
33. Vacher H, Yang J-W, Cerda O, Autillo-Touati A, Dargent B, Trimmer JS. Cdk-mediated phosphorylation of the Kvβ2 auxiliary subunit regulates Kv1 channel axonal targeting. J Cell Biol. 2011 Mar 7;192(5):813–24.
34. Liu W, Devaux JJ. Calmodulin orchestrates the heteromeric assembly and the trafficking of KCNQ2/3 (Kv7.2/3) channels in neurons. Mol Cell Neurosci. 2014 Jan;58:40–52.
35. Schafer DP, Jha S, Liu F, Akella T, McCullough LD, Rasband MN. Disruption of the Axon Initial Segment Cytoskeleton Is a New Mechanism for Neuronal Injury. J Neurosci. 2009 Oct 21;29(42):13242–54.
36. D'Este E, Kamin D, Göttfert F, El-Hady A, Hell SW. STED Nanoscopy Reveals the Ubiquity of Subcortical Cytoskeleton Periodicity in Living Neurons. Cell Rep. 2015 Mar;10(8):1246–51.
37. Xu K, Zhong G, Zhuang X. Actin, Spectrin, and Associated Proteins Form a Periodic Cytoskeletal Structure in Axons. Science. 2013 Jan 25;339(6118):452–6.
38. Lukinavičius G, Reymond L, D'Este E, Masharina A, Göttfert F, Ta H, et al. Fluorogenic probes for live-cell imaging of the cytoskeleton. Nat Methods. 2014 Jul;11(7):731–3.
39. Tam J, Merino D. Stochastic optical reconstruction microscopy (STORM) in comparison with stimulated emission depletion (STED) and other imaging methods. J Neurochem. 2015 Nov;135(4):643–58.
40. Vicidomini G, Bianchini P, Diaspro A. STED super-resolved microscopy. Nat Methods. 2018 Mar;15(3):173–82.
41. Blom H, Widengren J. Stimulated Emission Depletion Microscopy. Chem Rev. 2017 Jun 14;117(11):7377–427.
42. Kaech S, Banker G. Culturing hippocampal neurons. Nat Protoc. 2006 Dec;1(5):2406–15.
43. Non-Linear Least-Squares Minimization and Curve-Fitting for Python — Non-Linear Least-Squares Minimization and Curve-Fitting for Python [Internet]. [cited 2021 Jul 13]. Available from: https://lmfit.github.io/lmfit-py/
44. O'Connell KMS, Loftus R, Tamkun MM. Localization-dependent activity of the Kv2.1 delayed-rectifier K+ channel. Proc Natl Acad Sci U S A. 2010 Jul 6;107(27):12351–6.
45. Rivera C, Voipio J, Payne JA, Ruusuvuori E, Lahtinen H, Lamsa K, et al. The K+/Cl− co-transporter KCC2 renders GABA hyperpolarizing during neuronal maturation. Nature. 1999 Jan;397(6716):251–5.
46. Rivera C. Mechanism of Activity-Dependent Downregulation of the Neuron-Specific K-Cl Cotransporter KCC2. J Neurosci. 2004 May 12;24(19):4683–91.

47. Bading H, Ginty D, Greenberg M. Regulation of gene expression in hippocampal neurons by distinct calcium signaling pathways. Science. 1993 Apr 9;260(5105):181–6.
48. OpenCV: OpenCV modules [Internet]. [cited 2021 Aug 1]. Available from: https://docs.opencv.org/master/index.html
49. Welcome to Flask — Flask Documentation (2.0.x) [Internet]. [cited 2021 Aug 1]. Available from: https://flask.palletsprojects.com/en/2.0.x/
50. OpenCV: Image Segmentation with Watershed Algorithm [Internet]. [cited 2021 Aug 1]. Available from: https://docs.opencv.org/4.5.2/d3/db4/tutorial_py_watershed.html

Acknowledgments - I would like to give special regards to my supervisor, Hanne Borger Rasmussen, this research, and thesis would not have been possible without her exceptional support and guidance. I also thank the University of Copenhagen, Panum Institute, Faculty of Health and Medical Sciences for providing the necessary equipment and infrastructure. I thank and acknowledge the Core Facility for Integrated Microscopy (CFIM), Faculty of Health and Medical Sciences, University of Copenhagen for the imaging equipment and infrastructure. I wish to show my gratitude to Virginia Luque Fernández for sharing her knowledge and guiding me through the STED system. I thank Emil Arvedsen, Jannik Faliu, Pilar Martin Grande, Louse Menck Wildfang and Louise Koch for their help, guidance and teaching of protocols in the lab. Special thanks to Pablo Hernandez-Varas for confocal and STED microscopy training and guidance. Special thanks to Toon Heleven for teaching Python, HTML, and Javascript basics and his guidance on coding the used in-house software. I thank Elisa D'Este for sharing her knowledge on STED microscopy imaging and analysis. Finally, I thank Jelle Hendrix and Bert Brone for their feedback and comments throughout the internship period.

Authors contributions – HBR conceived and designed the research. SV performed experiments and data analysis and wrote the thesis with the initial guidance of HBR. JH provided feedback and guidance on the research.

SUPPLEMENT

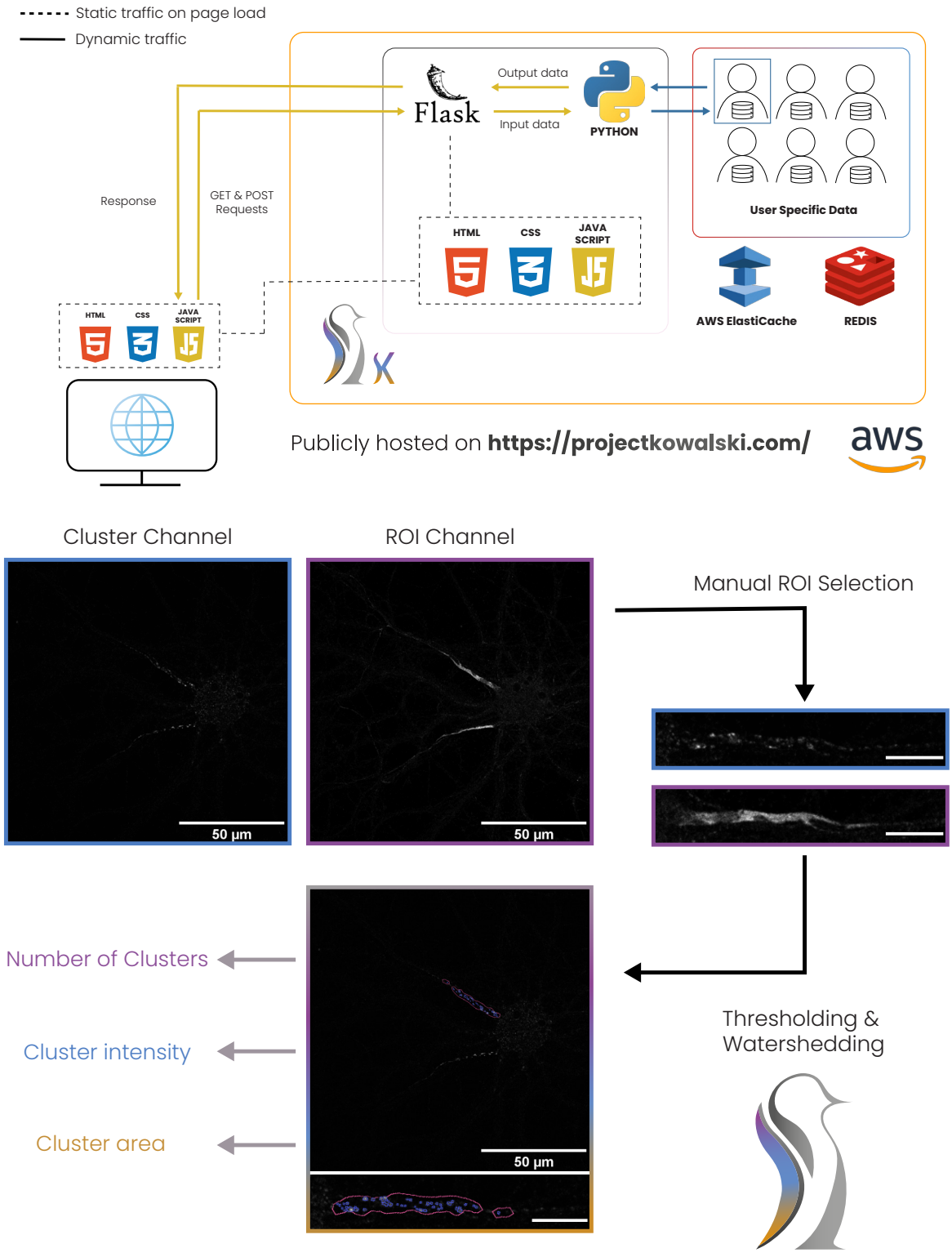

Supplement box 1: Technical description of in-house software built for Kv2.1 cluster analysis: Core Cluster Counter processes were built in Python 3.8. Most image processing (thresholding, gaussian blur, watershed) was written using OpenCV (48), an open-source library including multiple computer vision algorithms. Since image analysis is a visual process, it was vital to build a well-organized graphical user interface (GUI) to make the analysis easy to understand and less time-consuming. The GUI was build in browser compatible and widely used HTML5 (CSS3 for style

code) and Javascript for dynamic elements. Flask library was used for the easy communication between the core python code and the dynamic Javascript elements in the GUI (49). Flask works by translating GET & POST requests from the site into python compatible input data. In the opposite direction, Flask can translate python output data like created images, zip files, and datasheets into javascript compatible responses to easily display data in the GUI. Since the tool was already browser compatible, it was decided to push the code onto the web, hosted by amazon web services (AWS). A Redis server was set up to store all temporary user data in a secure location linked to a randomly generated user-specific universally unique identifier (UUID) to avoid cross-talk between users. For easy communication between the Redis server and the core python code, the Redis infrastructure was hosted on AWS ElastiCache. It was ensured that all user data was secure and inaccessible to other users or the server host and destroyed upon disconnect with the user.

In short, after uploading a .czi image, the user is asked to define a threshold where all the clusters are visible. An optional threshold can be set on a ROI channel (in this case, AnkG to define the AIS). Additionally, a manual ROI can be set to limit the analysis to a specific part of the image. Afterward, clusters are automatically separated using the watershed principle (50). This allows the tool to extract the number of clusters, average intensity in each cluster, and each cluster's pixel area.

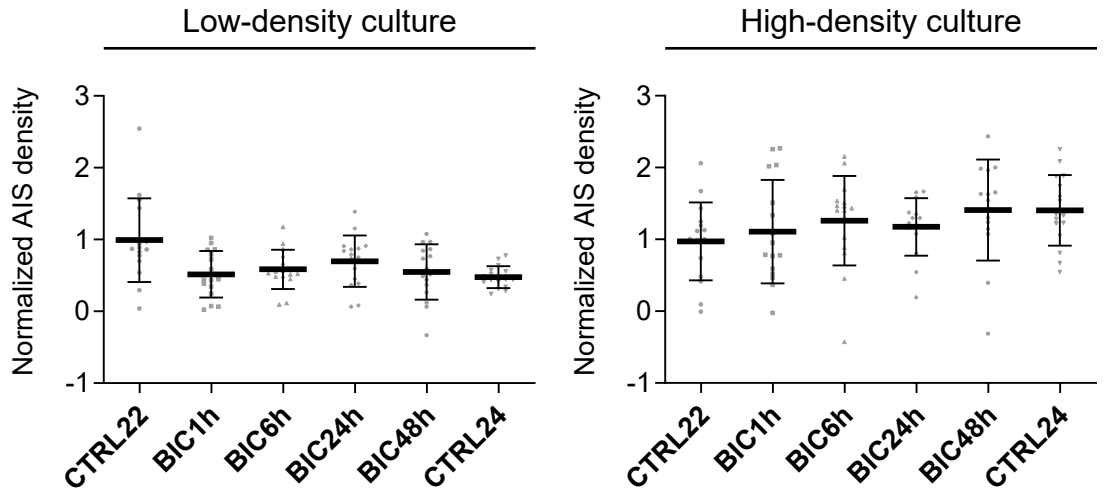

Supplement Figure 2: Kv1.1 immunofluorescent intensity after activity stimulation varied greatly between cultures. Normalized AIS densities of Kv1.1 in a time series of activity stimulation using BIC from two separate hippocampal neuron cultures resulted in two very different outcomes. A possible explanation for this derives from the cultures' overall cell density. Kv1.1 intensity seemed to go down in the low-density culture, while the opposite was observed in the high-density culture. Whether this effect is caused by BIC treatment was unsure as 24 DIV control data (CTRL24) also varies greatly between the cultures.

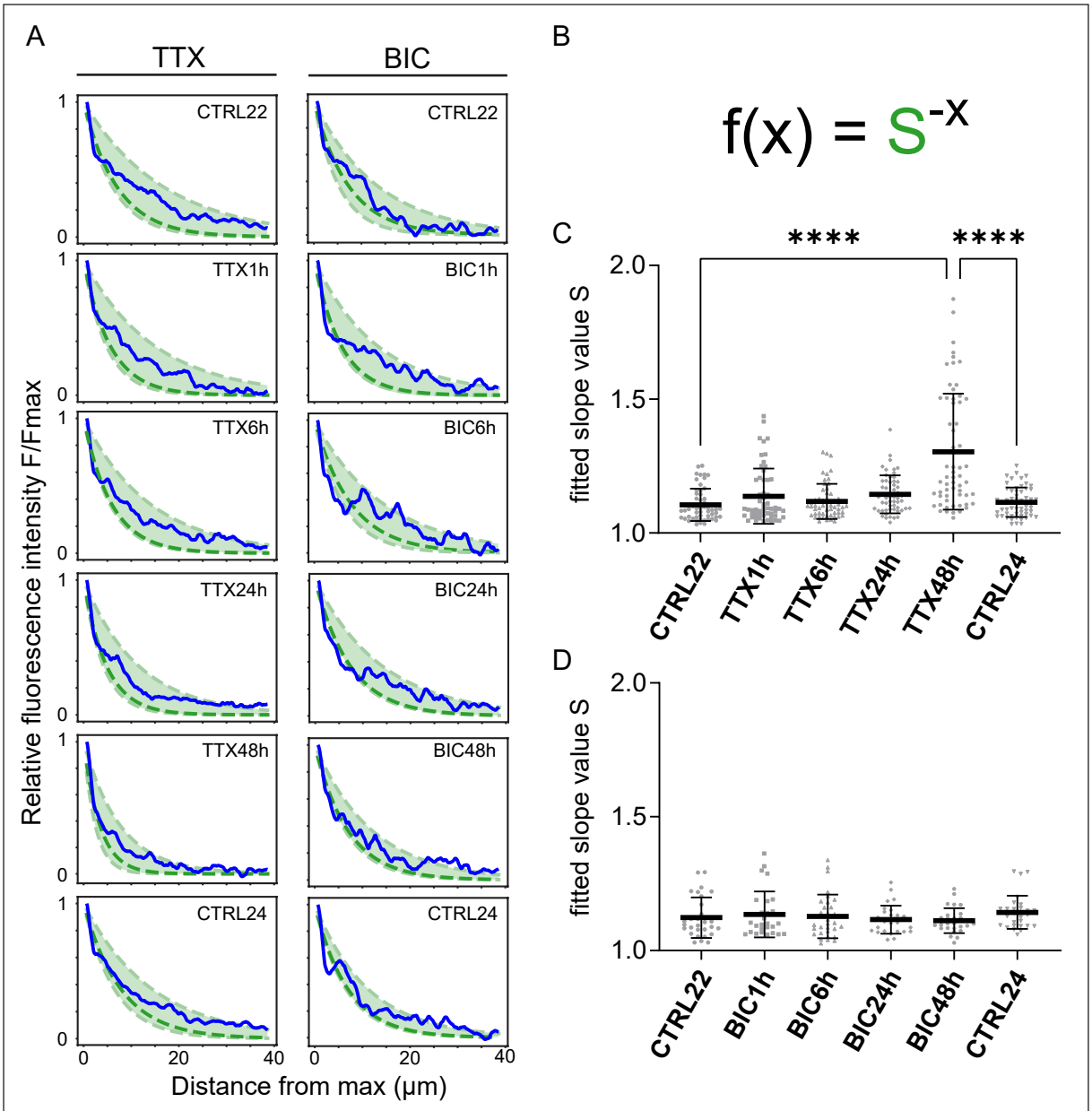

Supplement Figure 3: Kv1.1 end slope changes on activity manipulation. A) Relative intensity profiles from the max intensity (blue) and fitted curves (green). Dark green represents the mean fitted value of S, with light green being the interquartile range. B) Fitting model with S as the fitted parameter. C) Fitted slope parameter S for all conditions of an activity deprivation timeline. D) Fitted slope parameter S for all conditions of an activity deprivation timeline. Significance was determined by a Kruskal-Wallis test. Fitting was done in Python 3.8 using the Lmfit library (41). **** $P < 0.0001$.

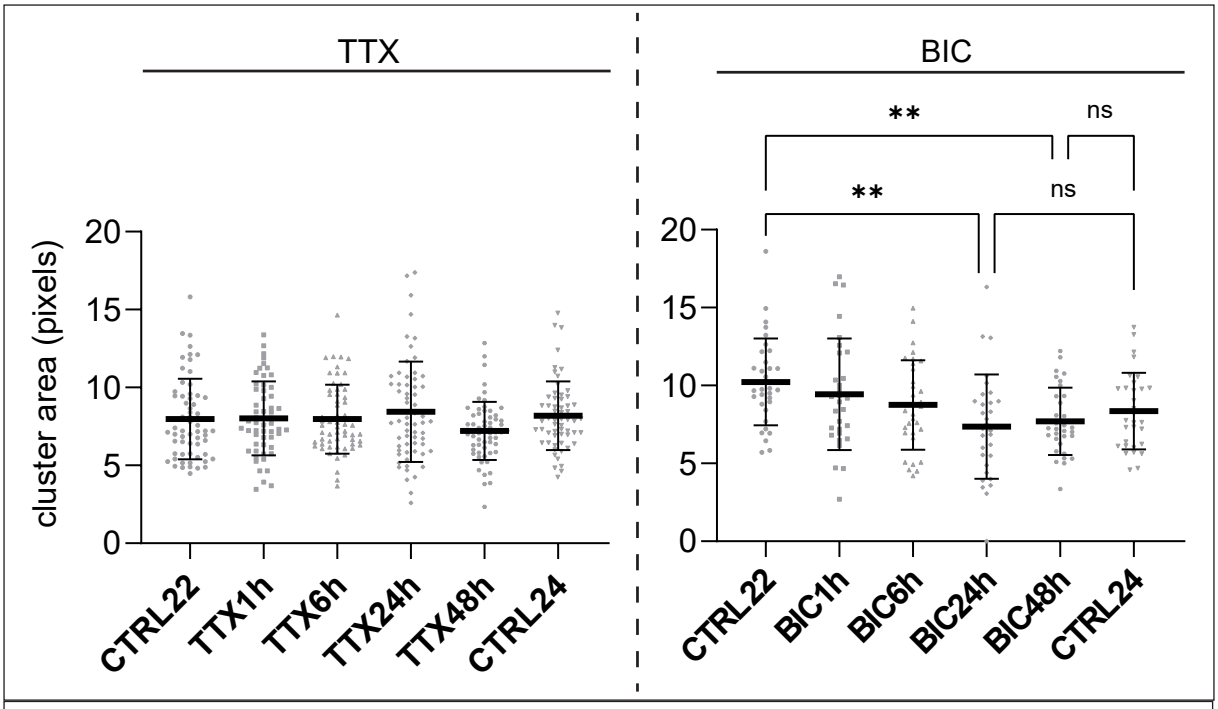

Supplement Figure 4: Effects of activity manipulation on Kv2.1 cluster characteristics: A) Average Kv2.1 cluster area in pixels over a time series of activity deprivation (TTX) and stimulation (BIC). Number of neurons; TTX time-series (n = 58-62 per condition), BIC time-series (n = 30-33). * $P < 0.05$, ** $P < 0.01$.

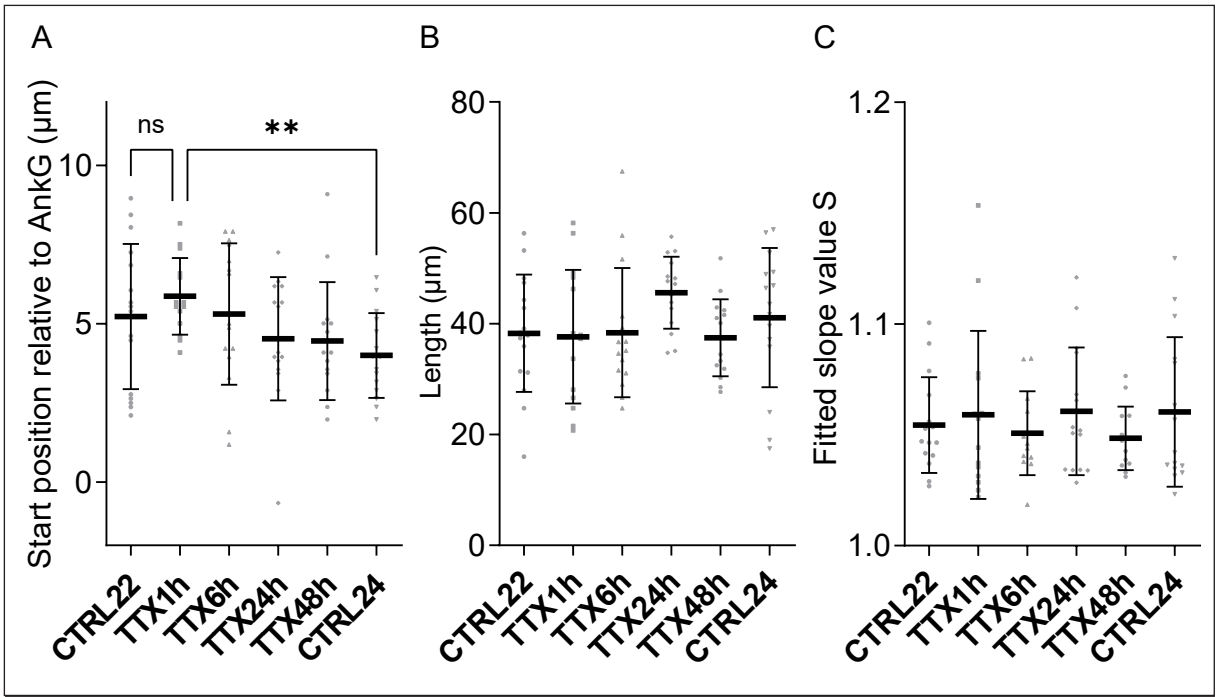

Supplement Figure 5: Effect of activity stimulation and deprivation on the localization of Kv7.2: A) Start position of Kv7.2 relative to the start position of AnkG along the axon. B) Length of Kv7.2 segments where the start position is defined by where the intensity profile rises above 33% of the max intensity for the first time, and the end position is defined by where a fitted end slope (S^{-x}) dips below 33% of the max intensity for the first time. Number of neurons; TTX time-series (n = 15-16 per condition), ** $P < 0.01$.

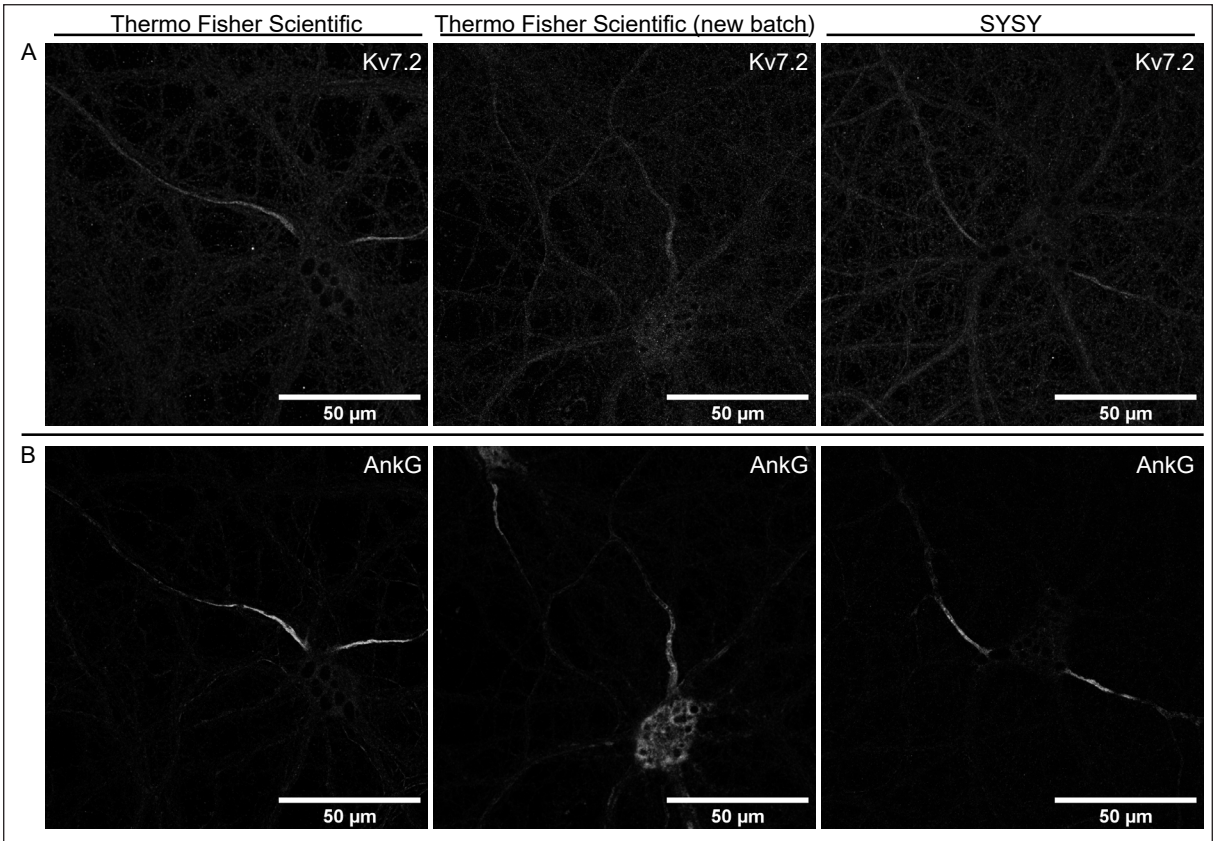

Supplement Figure 6: Comparison of multiple anti-Kv7.2 antibodies: A) Rat hippocampal 22 DIV neurons stained with rabbit anti-Kv7.2 (Thermo Fisher Scientific) on the left, a new batch of rabbit anti-Kv7.2 (Thermo Fisher Scientific) in the middle, and rabbit anti-Kv7.2 (SYSY) on the right B) Respective stainings with a mouse anti-AnkG antibody.